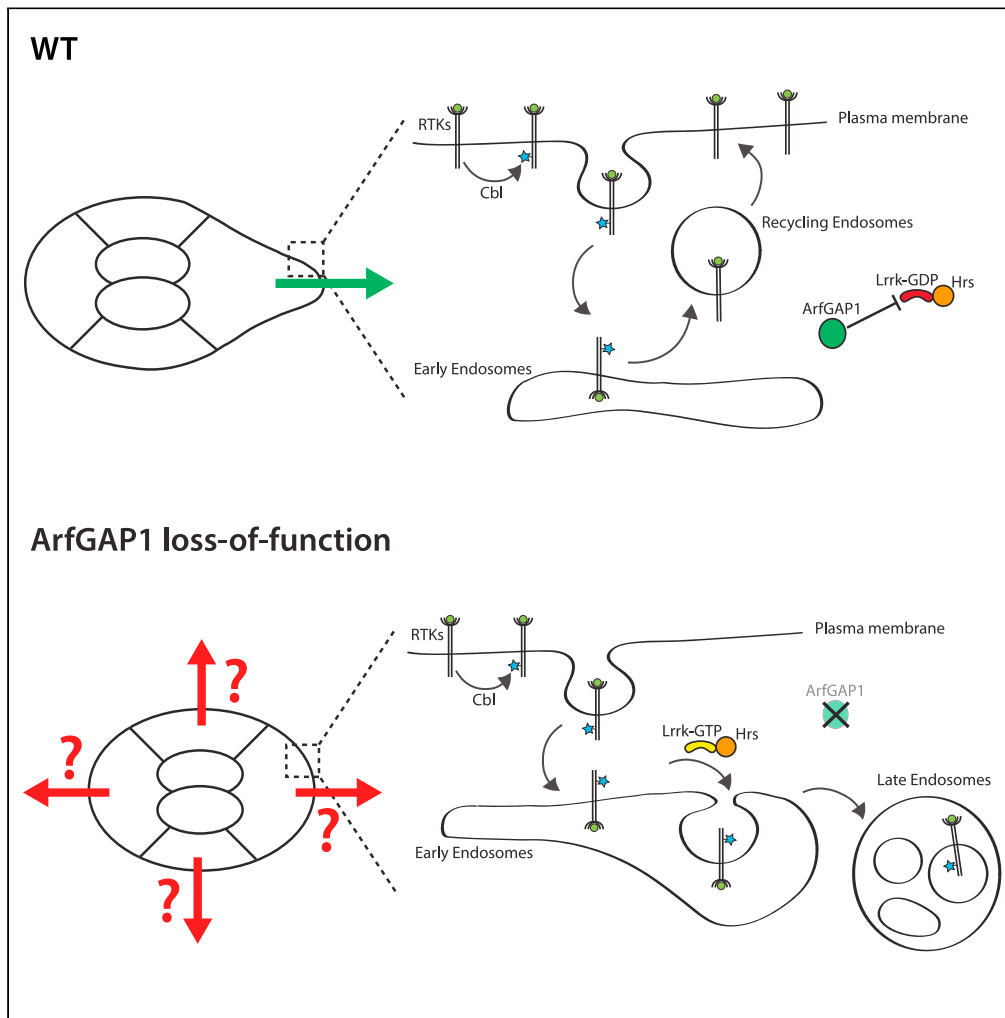


Article

ArfGAP1 regulates the endosomal sorting of guidance receptors to promote directed collective cell migration *in vivo*



Alison Boutet,  
Carlos Zeledon,  
Gregory Emery

gregory.emery@umontreal.ca

Highlights

ArfGAP1 is required for the directed migration of *Drosophila* border cells

The function of ArfGAP1 is GAP-dependent

ArfGAP1 regulates the sorting of guidance receptors in endosomes

ArfGAP1 negatively regulates Hrs and Lrrk



## Article

ArfGAP1 regulates the endosomal sorting of guidance receptors to promote directed collective cell migration *in vivo*Alison Boutet,<sup>1</sup> Carlos Zeledon,<sup>1</sup> and Gregory Emery<sup>1,2,3,\*</sup>

## SUMMARY

**Chemotaxis drives diverse migrations important for development and involved in diseases, including cancer progression. Using border cells in the *Drosophila* egg chamber as a model for collective cell migration, we characterized the role of ArfGAP1 in regulating chemotaxis during this process. We found that ArfGAP1 is required for the maintenance of receptor tyrosine kinases, the guidance receptors, at the plasma membrane. In the absence of ArfGAP1, the level of active receptors is reduced at the plasma membrane and increased in late endosomes. Consequently, clusters with impaired ArfGAP1 activity lose directionality. Furthermore, we found that the number and size of late endosomes and lysosomes are increased in the absence of ArfGAP1. Finally, genetic interactions suggest that ArfGAP1 acts on the kinase and GTPase Lrrk to regulate receptor sorting. Overall, our data indicate that ArfGAP1 is required to maintain guidance receptors at the plasma membrane and promote chemotaxis.**

## INTRODUCTION

Cell migration is a fundamental process that can take various forms. For example, cell migration can be directed or not. One example of directed cell migration is chemotaxis that happens through the binding of chemoattractant by guidance receptors.<sup>1</sup> Furthermore, cells can migrate either individually or collectively in groups of different sizes.<sup>2</sup> Chemotaxis and collective cell migration play fundamental roles during development.<sup>3</sup> Unfortunately, they are also mechanisms exploited by cancer cells to form metastasis.<sup>2</sup> Understanding how groups of cells sense and respond to chemotaxis gradients is of high importance. Border cell migration in the *Drosophila* egg chamber is among the most potent models to study collective cell migration and chemotaxis *in vivo*.<sup>4–7</sup>

The *Drosophila* egg chamber is composed of 15 large nurse cells and the oocyte, surrounded by follicle cells. The border cells derive from these somatic cells and form a small cluster of 6–10 cells that perform an anteroposterior invasive migration between the nurse cells toward the oocyte.<sup>6,7</sup> The oocyte secretes the ligands PVF1, Keren, and Spitz. They attract the border cells by activating two receptor tyrosine kinases (RTKs): the epidermal growth factor receptor (EGFR) and PVR, the sole orthologue of the platelet-derived growth factor receptor and the vascular endothelial growth factor receptor.<sup>8–11</sup> Upon binding to their ligands, the RTKs recruit the Rac guanine exchange factor (GEF) Vav to activate Rac and form protrusions in 1 or 2 cells at the leading edge of the cell cluster.<sup>12</sup> Rac activity and protrusion formation seem to be actively repressed in the other cells of the cluster through a mechanism involving the actin and plasma membrane binding protein Moesin, the cell-cell adhesion protein DE-cadherin, and Myosin II-mediated contractility.<sup>13–17</sup>

In previous work, we and others have shown that vesicular trafficking plays an important role in regulating border cell migration.<sup>14,18–24</sup> In particular, endocytosis and recycling were shown to regulate the level and the distribution of active RTKs at the plasma membrane and hence to be required for directed migration.<sup>18,19,22–24</sup> In mammals, the trafficking of RTKs was shown to be regulated by several means (reviewed in<sup>25</sup>). For example, the ubiquitination of the EGFR by the E3-ligase Cbl changes its trafficking in the endocytic pathway. Indeed, while ubiquitination is dispensable for the internalization of RTKs from the plasma membrane, it serves as a sorting signal in endosomes, where ubiquitinated RTKs interact with the ESCRT-0 complex, composed of Hrs and Stam. This leads to the sorting of RTKs into internal vesicles of

<sup>1</sup>Vesicular Trafficking and Cell Signalling Research Unit, Institute for Research in Immunology and Cancer (IRIC), Université de Montréal, P.O. Box 6128, Downtown Station, Montréal, QC H3C 3J7, Canada

<sup>2</sup>Department of Pathology and Cell Biology, Faculty of Medicine, Université de Montréal, Montréal, QC H3C 3J7, Canada

<sup>3</sup>Lead contact

\*Correspondence: [gregory.emery@umontreal.ca](mailto:gregory.emery@umontreal.ca)

<https://doi.org/10.1016/j.isci.2023.107467>



multivesicular bodies and, subsequently, to transport to late endosomes and lysosomes, where they are degraded. On the contrary, non-ubiquitinated receptors can be recycled to the plasma membrane. Accordingly, border cells mutant for *cbl* have increased levels of RTKs at the plasma membrane suggesting either that less receptors are endocytosed or that they are recycled instead of being degraded. Furthermore, Hrs and Stam loss-of-functions in *Drosophila* lead to an accumulation of active RTKs in endosomes.<sup>24</sup> Overall, this suggests that a mechanism similar to the regulation of EGFR in mammals is at play to eliminate ubiquitinated receptors in flies. In addition, the recycling of RTKs was also observed in border cells, to maintain active RTKs at the cortex. Accordingly, Rab GTPases regulating entry and recycling from endosomes (Rab4, Rab5 and Rab11), their regulators (the GEF Sprint and the GTPase activating proteins (GAPs) Evi5 and Rn-Tre) and their effectors (the exocyst complex) have also been involved in border cell migration.<sup>18,19,22,23</sup> However, the exact mechanism by which RTKs are sorted toward the different endocytic compartments during border cell migration is still unclear to our knowledge.

To increase our understanding of the regulation of vesicular trafficking in border cells, we have previously performed a candidate RNAi screen.<sup>20</sup> This screen was directed against Arf, Arf-like GTPases, and their regulators, as Arf GTPases are known to be involved in the sorting of cargoes into vesicles.<sup>26</sup> Despite several candidates inducing pleiotropic effects, as expected since Arf GTPases are required to form vesicles in the biosynthetic pathway,<sup>27,28</sup> we found that a few candidates induced specific phenotypes. For example, we found that the GAP Drongo was required to promote contractility at the onset of border cell migration.<sup>20</sup> In the present study, we focus on ArfGAP1. ArfGAP1 was originally shown to act as a GAP for Arf1.<sup>29</sup> As Arf1 is necessary for the formation of COPI-coated vesicles, ArfGAP1 was shown to be an essential regulator of their formation.<sup>30,31</sup> In *Drosophila*, the ArfGAP1 activity toward Arf1 was involved in eye pigmentation and rhabdomere biogenesis,<sup>32,33</sup> in blood cell homeostasis<sup>34</sup> and in epithelial tube expansion in the trachea.<sup>35</sup> Interestingly, the mammalian orthologue of ArfGAP1 was also shown to act as a GAP for Lrrk2.<sup>36,37</sup> Lrrk proteins have both a GTPase and kinase activity<sup>38</sup> and Lrrk2 is an important factor involved in the development of Parkinson's disease.<sup>39</sup> Here, we show that ArfGAP1 is required for the chemotaxis of border cells by maintaining active RTKs at the cell surface. This is achieved by regulating the endo-lysosomal pathway possibly through Lrrk, the sole Lrrk1 and Lrrk2 orthologue in flies, and the ESCRT-0 complex protein Hrs.

## RESULTS

### The GAP activity of ArfGAP1 is required for border cell migration

In previous work,<sup>20</sup> we have performed an RNAi screen to identify new regulators of collective cell migration among Arf and Arf-like GTPases, their GAPs and their GEFs. In this screen, we used the Gal4/UAS system to express the control dsRNA or dsRNAs targeting candidates specifically in border cells with the *c306*-Gal4 driver. ArfGAP1 caught our attention as its depletion impaired border cell migration, without inducing pleiotropic effects or disrupting the Golgi apparatus (Figures 1A, 1B, and S1A–S1C; <sup>20</sup>). To validate that the phenotype was not due to off-targets, we overexpressed a mCherry-tagged version of ArfGAP1 in depleted clusters. Although this construct is still targeted by the RNAi line, we observed a complete rescue of border cell migration (Figures 1A and 1B). To further confirm the specificity of the dsRNAs, we generated flies containing the *Drosophila pseudoobscura* orthologue of ArfGAP1 and found that its expression entirely rescued the phenotype induced by the depletion of ArfGAP1 (Figure S2A).

To confirm that the loss of ArfGAP1 blocks border cell migration, we generated a null mutant by using CRISPR/Cas9.<sup>40</sup> We isolated different deletions. Among these, the allele *ArfGAP1<sup>5</sup>* has a frameshift at amino acid 37 leading to a stop codon at position 75. Consequently, *ArfGAP1<sup>5</sup>* has lost the catalytic arginine at position 50<sup>41</sup> and should be non-functional (Figure 1C). *ArfGAP1<sup>5</sup>* is homozygous viable and induces a delayed border cell migration that was similar, but slightly inferior to the depletion by RNAi (Figure 1B). The weaker phenotype observed in the mutant is possibly due to compensatory mechanisms that are not required for survival when ArfGAP1 is depleted solely in border cells with the Gal4/UAS system. To determine if *ArfGAP1<sup>5</sup>* acts as a genetic null, we crossed it to a deficiency line covering *ArfGAP1* (*Df(3L)BSC730*). The phenotype observed in *ArfGAP1<sup>5</sup>/Df(3L)BSC730* was identical to homozygous *ArfGAP1<sup>5</sup>*, indicating that *ArfGAP1<sup>5</sup>* is a null allele. As for the depletion of ArfGAP1, we found that the expression of the *Drosophila pseudoobscura* homolog of ArfGAP1 rescued the mutant phenotype (Figure S2A).

To determine if the GAP activity of ArfGAP1 is required for border cell migration, we generated a GAP inactive form of ArfGAP1 (*ArfGAP1<sup>R50Q</sup>*, Figure 1C) and expressed it in ArfGAP1 depleted clusters. We found

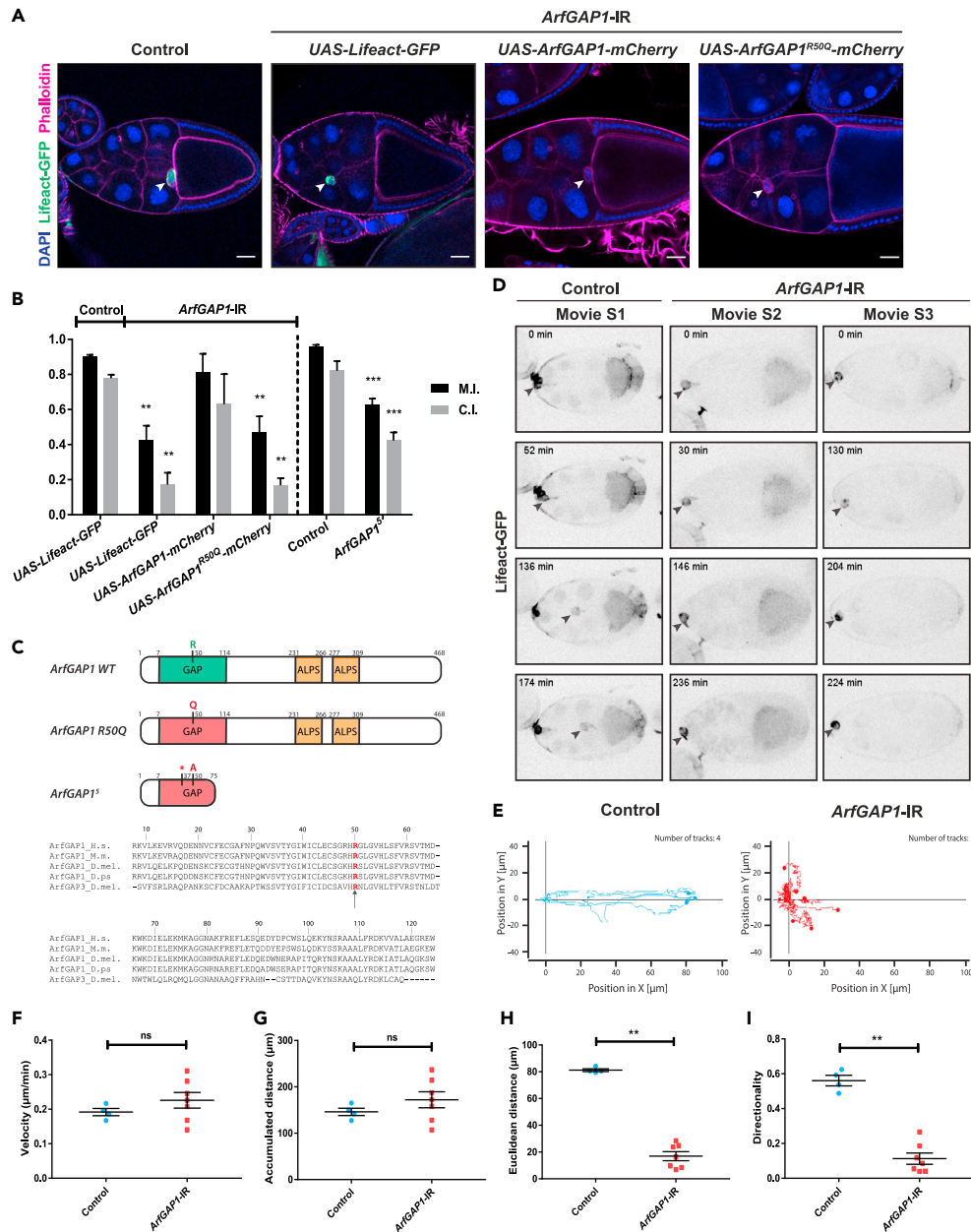


**Figure 1. *ArfGAP1* is required for the directional migration of border cells**

(A) Representative images of a control stage 10 egg chamber and stage 10 egg chambers expressing the *ArfGAP1* RNA interference (*ArfGAP1-IR*) with the indicated constructs. Arrowheads indicate the localization of the border cell cluster. Scale bar: 30  $\mu\text{m}$ .

(B) Migration Indexes (M.I.) and Completion Indexes (C.I.) (see STAR Methods) for the different genotypes indicated. Error bars are SEM ( $82 \leq n \leq 312$  clusters;  $N = 3$  experiments; \*\*:  $p < 0.01$ , \*\*\*:  $p < 0.001$ , \*\*\*\*:  $p < 0.0001$ , compared to Control *UAS-Lifeact-GFP* and to Control, One-way ANOVA test).

(C) Scheme of *ArfGAP1* WT, *ArfGAP1*<sup>R50Q</sup> and *ArfGAP1*<sup>5</sup> protein sequences. \*: change in sequence compared to WT. Alignment of the protein sequences of Human (H.s.) *ArfGAP1*, Mouse (M.m.) *ArfGAP1*, *Drosophila melanogaster* (D.mel.) and *Drosophila pseudoobscura* (D.ps) *ArfGAP1* and *Drosophila* (D.mel.) *ArfGAP3*.

(D) Representative images from time-lapse recordings of the migration of border cells expressing Lifeact-GFP in control egg chamber (left, Video S1) or after *ArfGAP1* depletion (middle, right, Videos S2 and S3). Arrowheads indicate the localization of the border cell cluster.

**Figure 1. Continued**

(E) Traces from time-lapse recordings of border cell migration in control egg chambers (left) or after depletion of ArfGAP1 (right).

(F–I) Mean velocity, mean accumulated distance, mean Euclidian distance, and mean directionality from time-lapse recordings of control and ArfGAP1 depleted clusters. Error bars are SEM ( $4 \leq n \leq 7$  clusters; ns: not significant ( $p > 0.05$ ), \*\*:  $p < 0.01$ , Mann-Whitney test).

that the expression of the catalytic inactive ArfGAP1 was unable to rescue ArfGAP1 depletion, showing that the GAP activity is necessary for ArfGAP1's function in border cells (Figures 1A and 1B). Interestingly, over-expressing ArfGAP1 or expressing ArfGAP1<sup>R50Q</sup> did not affect border cell migration (Figure S2B).

**ArfGAP1 is necessary to maintain the directionality of border cell migration**

To gain information, we compared time-lapse recordings of control clusters to clusters depleted for ArfGAP1. Contrary to control clusters (Video S1, Figure 1D) that perform a direct migration toward the oocyte, we observed that clusters depleted of ArfGAP1 either (1) seemed active and migrated on very short distances, but were not progressing, possibly by being unable to maintain directionality and undergoing a shuffling and tumbling behavior similar to control clusters probing for directionality<sup>42</sup> (Video S2, Figure 1D), or (2) migrated on longer distance before changing directionality toward the wrong path (Video S3, Figure 1D). However, subsequent analysis of the ArfGAP1 loss-of-function showed homogeneous phenotypes (see below), suggesting that both behaviors might originate from the same defects. We always saw a normal number of protrusions (Figure S2C) and cohesive clusters. Accordingly, we found that the active, phosphorylated form of Moesin that is required to coordinate the cells of the cluster<sup>13,14</sup> is also normally distributed at the periphery of the cluster after the depletion of ArfGAP1 (Figures S1D–S1E). We quantified time-lapse recordings of clusters depleted of ArfGAP1 and found that the mean velocity of depleted clusters was 0.226  $\mu\text{m}/\text{min}$ , similar to control cluster (0.192  $\mu\text{m}/\text{min}$ ), but the directionality and the total displacement for the course of the recording were dramatically reduced (Figures 1D–1H).

Loss of directionality can be due to abnormal polarization of the cluster. Hence, we monitored the distribution of the polarity proteins Discs Large and Bazooka (Par3) that are required for the spatial organization of the cluster<sup>43–45</sup> and found that they were unaffected (Figures S1F–S1G). The migration phenotype we observed was similar to the loss-of-function of DE-cadherin which is necessary for the border cell – nurse cell interaction, to maintain the cohesion in the cluster and to ensure directional migration.<sup>46,47</sup> We found that DE-cadherin is normally distributed in ArfGAP1 depleted clusters (Figure S2H).<sup>20</sup> Similarly, another adhesion protein, Fasciclin III<sup>48</sup> was also unaffected by the depletion of ArfGAP1 (Figure S1I). Overall, our data indicate that most of the determinants required for border cell migration are unaffected by the depletion of ArfGAP1. Hence, we decided to further investigate the exact molecular mechanism regulated by ArfGAP1 in border cells.

Since directionality is lost but polarity is normal, we hypothesized that the capacity of ArfGAP1 depleted clusters to sense the gradient of RTK ligands guiding border cell migration is impaired. Indeed, clusters having impaired RTK activity are unable to sense the ligand gradient,<sup>49</sup> and clusters migrating in egg chambers expressing uniform levels of PVF1 migrate abnormally, displaying increased shuffling behavior.<sup>42</sup>

**Depletion of ArfGAP1 leads to an accumulation of active RTKs in the endo-lysosomal pathway**

To test the hypothesis that ArfGAP1 regulates RTKs, we monitored the distribution of active RTKs with the monoclonal antibody 4G10 that recognizes phosphorylated Tyrosines (pTyr).<sup>18,19,24</sup> To ensure consistency, our analyses were performed on egg chambers at stage 9, which contained clusters that were rounded and either detached or close to detaching from the follicular epithelium (see STAR Methods). While in control conditions active RTKs are predominantly found at the cortex, after depletion of ArfGAP1 or in homozygous ArfGAP1<sup>5</sup> mutant egg chambers, the pTyr signal accumulated in intracellular, vesicular-like structures (Figures 2A and 2B). Concomitantly, we observed a decrease of active RTKs at the plasma membrane at the migration front (Figure 2C). To test if this redistribution is due to the loss of the GAP activity of ArfGAP1, we performed rescue experiments. We found that the expression of wildtype ArfGAP1 in ArfGAP1 depleted clusters restores the normal localization of active RTKs that are now excluded from endosomal structures and found at the plasma membrane. On the contrary, the expression of the catalytic inactive form of ArfGAP1 did not rescue the phenotype indicating that the catalytic activity of ArfGAP1 is important to maintain active RTKs at the plasma membrane (Figures 2A–2C).

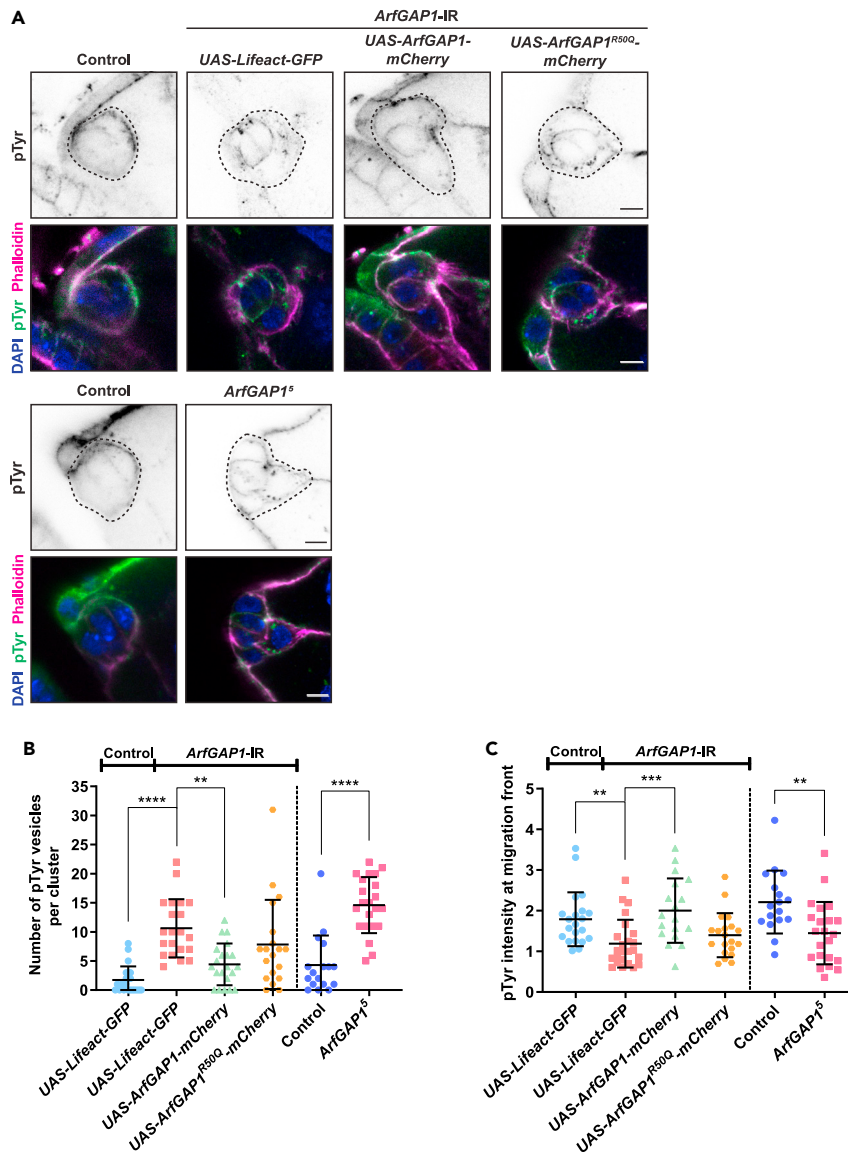


**Figure 2. ArfGAP1 depletion mis-localizes active RTKs in vesicular structures**

(A) Representative images of border cell clusters at onset of migration with the indicated genotype, labeled with the anti-pTyr antibody 4G10. Scale bar: 5  $\mu$ m. Clusters are delineated by a dotted line.

(B) Quantification of the number of pTyr positive vesicles per cluster in the indicated conditions. Error bars are SEM ( $17 \leq n \leq 24$  clusters; N = 3 experiments; \*\*,  $p < 0.01$ , \*\*\*\*,  $p < 0.0001$ , compared to *ArfGAP1-IR UAS-Lifeact-GFP*, Kruskal-Wallis and compared to Control, Mann-Whitney test).

(C) Quantification of the plasma membrane mean intensity of the pTyr signal at the migration front (see STAR Methods) in the indicated conditions. Error bars are SEM ( $17 \leq n \leq 24$  clusters; N = 3 experiments; \*\*,  $p < 0.01$ , \*\*\*\*,  $p < 0.001$ , compared to *ArfGAP1-IR UAS-Lifeact-GFP*, Kruskal-Wallis and compared to Control, Mann-Whitney test).

Next, we investigated in which compartment active RTKs were trapped after ArfGAP1 depletion by co-staining border cells with pTyr and markers of various endocytic compartments. First, we observed that active RTKs co-localized with large structures labeled with the endosomal marker GFP-myc2xFYVE<sup>50</sup> (Figure 3A). In *Drosophila*, FYVE marks both early and late endosomes.<sup>50,51</sup> Interestingly, active RTKs were found inside structures surrounded by FYVE. This suggested that active RTKs were accumulating in multivesicular bodies or in late endosomes. Accordingly, we found that pTyr did not co-localize with markers of the early endosome (GFP-Rab5,<sup>50</sup>) nor with GFP-Sec15, a marker of the recycling endosomes<sup>52</sup> (Figures 3B and 3C). However, we found that pTyr accumulated inside GFP-Rab7-positive structures, possibly in intraluminal vesicles

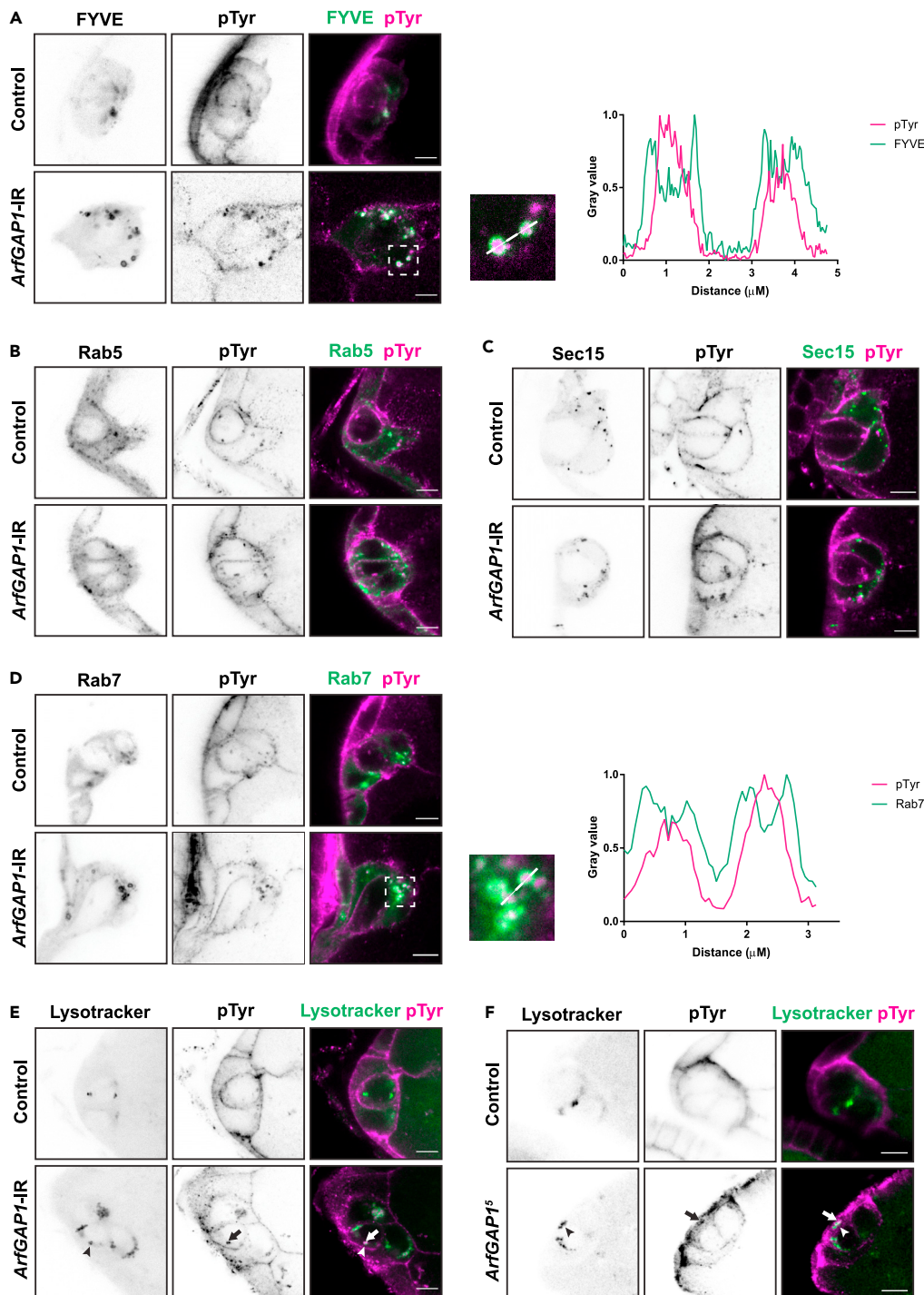


**Figure 3. Active RTKs (pTyr) accumulate in late endosomes after the depletion of ArfGAP1**

(A) Co-labeling of pTyr by immunofluorescence and endosomes (marked with GFP-myc2xFYVE) in control and ArfGAP1 depleted clusters at onset of migration. On the right, the high magnification image and the quantification of fluorescence by “line-scan” along a line that span over two puncta reveal that the pTyr signal is inside FYVE-positive vesicles. Scale bar: 5  $\mu\text{m}$ .

(B) Co-labeling of pTyr and early endosomes (GFP-Rab5) and (C) co-labeling of pTyr with recycling vesicles (GFP-Sec15) show no obvious overlap in control and ArfGAP1 depleted clusters at onset of migration. Scale bar: 5  $\mu\text{m}$ .

**Figure 3. Continued**

(D) Co-labeling of pTyr with the late endosomal marker GFP-Rab7 in control and ArfGAP1 depleted clusters at onset of migration. On the right, the high magnification image and the quantification of fluorescence by “line-scan” reveal that the pTyr signal is inside Rab7-positive vesicles in ArfGAP1-depleted clusters. Scale bar: 5  $\mu$ m.

(E) Co-labeling of pTyr with LysoTracker in control clusters, after depletion of ArfGAP1 or (F) in homozygous *ArfGAP1<sup>5</sup>* clusters at onset of migration. Scale bar: 5  $\mu$ m. Arrowheads and arrows indicate the localization of LysoTracker and pTyr vesicles respectively that are juxtaposed.

(Figure 3D). Co-labeling with the lysosomal marker LysoTracker showed that the pTyr signal was not found inside lysosomes, but frequently juxtaposed to lysosomal structures (Figure 3E). We hypothesize that RTKs are degraded when entering lysosomes and thus cannot be detected in them. We found a very similar distribution of active RTKs in *ArfGAP1<sup>5</sup>* homozygous egg chambers (Figure 3F). Altogether, these data suggest that active RTKs are overly targeted in the degradative pathway in the absence of ArfGAP1.

**ArfGAP1 regulates the degradative pathway**

Furthermore, we observed that the apparent GFP-Rab7 signal was increased in clusters depleted for ArfGAP1 (Figure 3D). We confirmed this observation by quantifying the mean intensity of the GFP-Rab7 signal at the onset of migration (Figure 4A). Correlating with our observation that active RTKs accumulate in late endosomes, we also found a significant increase of the pTyr signal inside Rab7 vesicles when ArfGAP1 is depleted (Figure 4B). To document a possible increase of the endo-lysosomal degradative pathway, we quantified the size of late endosomes and lysosomes as marked by Rab7 and LysoTracker respectively and we found a significant increase after ArfGAP1 depletion (Figures 4C and 4D). However, we did not detect any change in the positioning of Rab7 vesicles (Figure S2D). Moreover, the number of LysoTracker vesicles increased significantly in that condition (Figure 4E). The recycling endosome, labeled with GFP-Sec15, was unaffected (Figure S2E), suggesting that the effect was specific to the degradative pathway. To verify that the dysregulation of late endosomes and lysosomes was indeed due to the loss of ArfGAP1, we measured the size and the number of lysosomes in homozygous *ArfGAP1<sup>5</sup>* clusters. We also observed a similar increase of the number and the size of lysosomes in *ArfGAP1<sup>5</sup>* mutants (Figures 4D and 4E). These data show that ArfGAP1 regulates the degradative pathway.

**The ArfGAP1 phenotype is rescued by the co-depletion of Lrrk or Hrs**

Our findings suggest that ArfGAP1 inhibits the degradative pathway and the degradation of RTKs. In ArfGAP1 loss of function, RTKs would thus be overly degraded (Figure 4F). To determine the molecular mechanism regulating the sorting of RTKs that is regulated by ArfGAP1, we used genetic interactions. In control conditions, a pool of RTKs is ubiquitinated by the E3 ubiquitin ligase Cbl, which promotes their endocytosis and degradation.<sup>24</sup> We hypothesize that in ArfGAP1 depleted cluster, most of the ubiquitinated RTKs are now targeted into the degradative pathway. If our hypothesis is accurate, depleting Cbl may rescue the ArfGAP1 phenotype by reducing the endocytosis and degradation of RTKs. We found that Cbl co-depletion does not rescue border cell migration in ArfGAP1 depleted clusters (Figure 4G). As depletion of Cbl induces a migration phenotype *per se*, the absence of genetic interaction between ArfGAP1 and Cbl does not allow us to conclude that ArfGAP1 and Cbl act independently. However, this result suggests that the ArfGAP1 migration phenotype is not entirely dependent on the ubiquitination of RTKs.

Next, to gain insight into the mechanism by which ArfGAP1 regulates the localization of active RTKs, we searched for potential substrates of ArfGAP1 in the literature. ArfGAP1 was shown to act as a GAP on Arf1 and Lrrk2.<sup>29,36,37</sup> In previous work, we found that Arf1 depletion disrupts the Golgi apparatus.<sup>20</sup> On the contrary, the depletion of ArfGAP1 has no impact on the Golgi, as labeled by a GFP fusion to the trans-Golgi enzyme  $\beta$ 1,4-galactosyltransferase 1 (GalT)<sup>35</sup> (Figures S1A–S1C). From this, we concluded that it is unlikely that ArfGAP1 acts through Arf1 to regulate border cell migration. On the other hand, Lrrk1 was shown in mammals to promote the transport of EGFR from early to late endosomes by binding to Hrs and Stam, two components of the ESCRT-0 complex.<sup>53,54</sup> In *Drosophila*, there is a single Lrrk1 and Lrrk2 orthologue (Lrrk). Hence, it is possible that in the absence of ArfGAP1, Lrrk is overactivated and promotes the trafficking of RTKs into late endosomes and lysosomes through Hrs (Figure 4F). To test this, we used genetic interactions. We rationalized that if the depletion of ArfGAP1 increases Lrrk activity, the co-depletion of ArfGAP1 and Lrrk should restore migration. Accordingly, we found that the ArfGAP1 phenotype is rescued by the co-depletion of Lrrk (Figure 4G). Similarly, we co-depleted Hrs and ArfGAP1 and observed a rescue of the migration phenotype (Figure 4G). Furthermore, levels of pTyr at the membrane were restored and accumulation of pTyr in endosomes was reduced after co-depletion of ArfGAP1 with either Lrrk or Hrs (Figures 4H and 4I). To determine if ArfGAP1 regulates the localization of Hrs and Lrrk, we monitored their distribution in ArfGAP1 depleted clusters and did

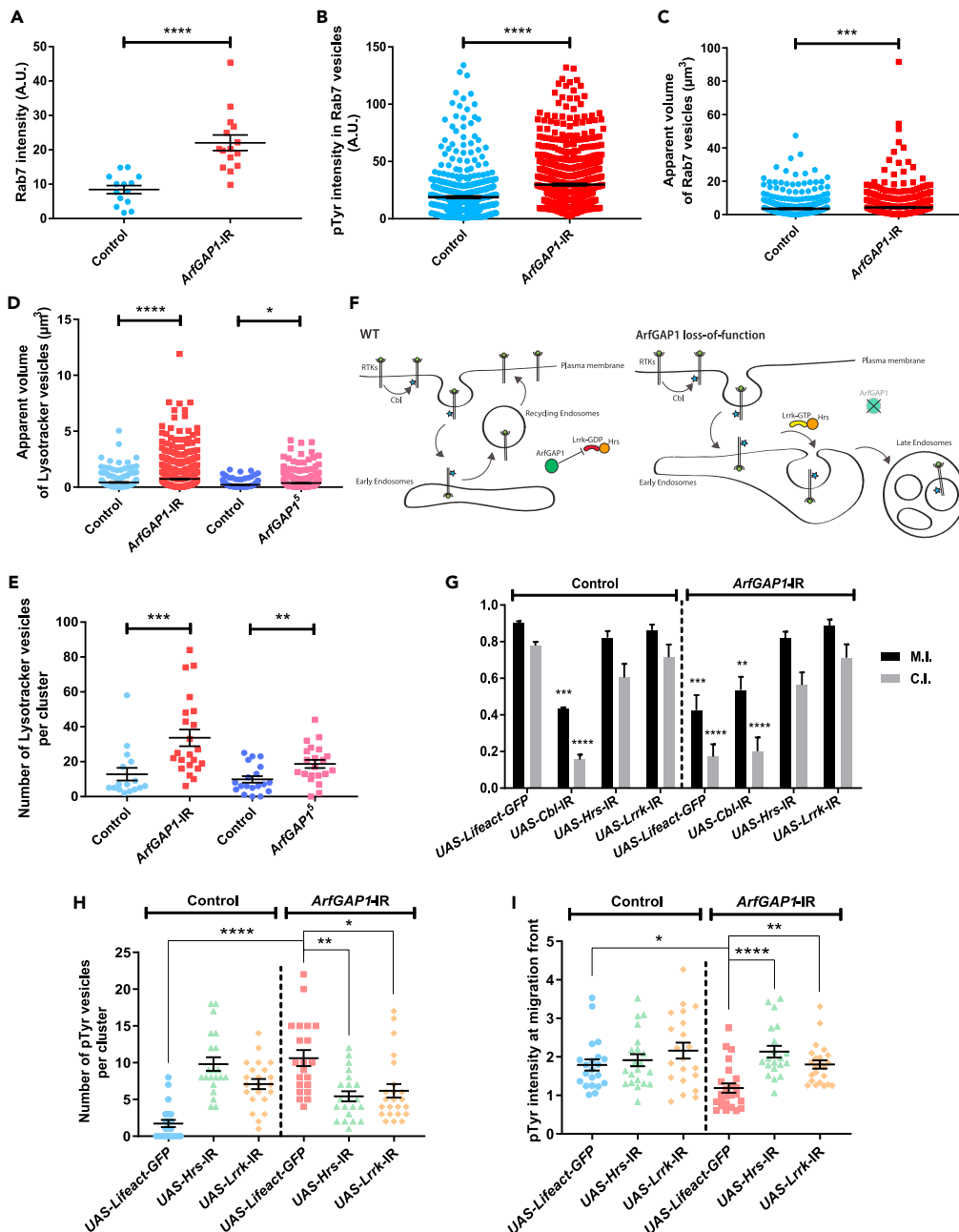


**Figure 4. ArfGAP1 regulates the homeostasis of the endo-lysosomal degradative pathway and interact genetically with Lrrk and Hrs**

(A) Quantification of the GFP-Rab7 intensity in control cluster and after depletion of ArfGAP1. Error bars are SEM ( $14 \leq n \leq 15$  clusters;  $N = 3$  experiments; \*\*\*\*:  $p < 0.0001$ , Mann-Whitney test).

(B) Intensity of the pTyr signal within Rab7-positive structures in control clusters and after depletion of ArfGAP1. Error bars are SEM ( $639 \leq n \leq 856$  vesicles;  $N = 3$  experiments; \*\*\*\*:  $p < 0.0001$ , Mann-Whitney test).

(C) Volume covered by Rab7-positive vesicles in control clusters and after depletion of ArfGAP1. Error bars are SEM ( $639 \leq n \leq 856$  vesicles;  $N = 3$  experiments; \*\*\*:  $p < 0.001$ , Mann-Whitney test).

(D) Volume covered by LysoTracker positive vesicles in control clusters, after depletion of ArfGAP1 and in homozygous ArfGAP1<sup>5</sup> egg chambers. Error bars are SEM ( $188 \leq n \leq 750$  vesicles;  $N = 3$  experiments; \*:  $p < 0.05$ , \*\*\*:  $p < 0.001$ , Kruskal-Wallis test).

(E) Number of LysoTracker positive vesicles in control clusters, after depletion of ArfGAP1 and in homozygous ArfGAP1<sup>5</sup> egg chambers. Error bars are SEM ( $16 \leq n \leq 22$  clusters;  $N = 3$  experiments; \*\*:  $p < 0.01$ , \*\*\*:  $p < 0.001$ , Kruskal-Wallis test).

(F) Proposed model depicting how ArfGAP1 regulates the trafficking of RTKs. Stars indicate ubiquitination.

**Figure 4. Continued**

(G) Migration and completion indexes of border cell migration in the indicated conditions. Error bars are SEM ( $113 \leq n \leq 312$  clusters;  $N = 3$  experiments; \*\*:  $p < 0.01$ , \*\*\*:  $p < 0.001$ , \*\*\*\*:  $p < 0.0001$ , compared to Control UAS-*Lifeact-GFP*, One-way ANOVA test).

(H) Quantification of the number of pTyr positive vesicles per cluster in the indicated conditions. Error bars are SEM ( $20 \leq n \leq 24$  clusters;  $N = 3$  experiments; \*:  $p < 0.05$ , \*\*:  $p < 0.01$ , \*\*\*\*:  $p < 0.0001$ , compared to *ArfGAP1-IR* UAS-*Lifeact-GFP*, Kruskal-Wallis test).

(I) Quantification of the plasma membrane mean intensity of the pTyr signal at the migration front (see STAR Methods) in the indicated conditions. Error bars are SEM ( $20 \leq n \leq 24$  clusters;  $N = 3$  experiments; \*:  $p < 0.05$ , \*\*:  $p < 0.01$ , \*\*\*\*:  $p < 0.0001$ , all p values shown are compared to *ArfGAP1-IR* UAS-*Lifeact-GFP*, Kruskal-Wallis test).

not see any difference compared to control (Figures S2H and S2I). Overall, our data suggests that *ArfGAP1* acts on *Lrrk* to inhibit the *Hrs*-mediated sorting of RTKs into the endo-lysosomal degradative pathway and their subsequent degradation.

**DISCUSSION**

Chemotaxis plays fundamental roles during development and in diseases such as cancer progression. During border cell migration, vesicular trafficking was shown by us and others to spatially control the distribution of the receptors responsible for chemotaxis. A recent screen performed in our laboratory identified new regulators of border cell migration including two Arf GAPs: *Drongo* and *ArfGAP1*.<sup>20</sup>

Here, we focused on *ArfGAP1*, which has been shown to act as a GAP on *Arf1*<sup>29</sup> and on *Lrrk2*.<sup>36,37</sup> Our findings suggest that *ArfGAP1* acts on *Lrrk* in border cells. *Lrrk* proteins are composed of both a kinase and a GTPase domain. Mammals have two *Lrrks* (*Lrrk1* and *Lrrk2*) that were shown to phosphorylate GTPases of the Rab family to modulate their interactions with specific effectors.<sup>55</sup> For example, *Lrrk1*, *Lrrk2* and *Drosophila* *Lrrk* were shown to regulate Rab7.<sup>55–58</sup> Phosphorylation of Rab7 by *Lrrk1* modulates its bindings to its effector RILP, that links Rab7 to dynein and regulates the positioning of late endosomes within the cell.<sup>57</sup> Accordingly, the expression of a *Lrrk* gain-of-function in *Drosophila* follicle cells inhibits the perinuclear accumulation of Rab7-positive puncta and increases the size of late endosomes and lysosomes in a Rab7-dependent mechanism.<sup>58</sup> Hence, it is appealing to hypothesize that Rab7 is a key target of *Lrrk* in border cells. This would need to be tested in detail.

Interestingly, mammalian *Lrrk1* was shown to regulate the transport of EGFR from early to late endosomes.<sup>53,54,57</sup> In particular, *Lrrk1* can interact with EGFR and the ESCRT-0 constituents *Hrs* and *Stam* in early endosomes.<sup>54</sup> Our work suggests that in border cells, *ArfGAP1* constrains the activity of *Lrrk* to inhibit the ESCRT-0-mediated sorting of RTKs into multivesicular bodies and the degradative pathway. Combined with these previous studies, our work suggests that *ArfGAP1* controls the endosomal sorting of RTKs through its GAP activity toward *Lrrk* that phosphorylates Rab7 and possibly other Rab proteins or regulates *Hrs*. Our model also suggests that the recycling of RTKs is promoted in the presence of *ArfGAP1* (Figure 4F). In the context of border cell migration, *ArfGAP1* thus plays an important role in maintaining active RTKs at the plasma membrane, and this ensures the proper guidance of border cells. It is interesting to speculate that *ArfGAP1* and *Lrrk* are regulators of the trafficking of RTKs in various contexts. As RTKs are required for various processes during development, tissue homeostasis and in the development of cancers, understanding the mechanism of action of *ArfGAP1* and *Lrrk* on RTKs is important.

An unexpected finding was the increase in late endosomes and lysosomes in *ArfGAP1* loss of function conditions. This suggests that normal levels of *ArfGAP1* are required to maintain the entire degradative pathway to its basal level. It would be important to address in future work if this role of *ArfGAP1* is cell specific to border cells or acts as a general mechanism for lysosomal homeostasis. Furthermore, it would be interesting to determine if *ArfGAP1* affects the protein levels of other transmembrane. In border cells, we observed that it does not reduce DE-cadherin levels at the cortex (Figure S1H),<sup>20</sup> demonstrating that some cargoes are still normally recycled. Furthermore, the recycling endosome compartment seems morphologically normal in *ArfGAP1* loss of function (Figures 3C and S1I). Overall, this suggests that the stimulation of the degradative pathway in *ArfGAP1* loss of function is not due to an impairment of the recycling pathway. Indeed, if this would be the case, we would anticipate an atrophy of the recycling pathway.

Positive feedback loops have long been proposed as a mechanism to transform a shallow extracellular gradient into a strong intracellular gradient, including during border cell migration.<sup>23,24</sup> Indeed, a positive

feedback loop might be an efficient way of transforming a signaling cue into a robust, directed response. As we found that ArfGAP1 regulates RTKs maintenance at the plasma membrane, it would be interesting to determine if it is part of a feedback loop that would be more active in the leader cell than in follower cells, and hence would reinforce the response to extracellular signals.

### Limitations of the study

In this study, we use genetic interactions to show that the role of ArfGAP1 depends on its GAP domain, and acts through Lrrk, in accordance with previous work in other models.<sup>36,37</sup> Although we demonstrate that the GAP activity of ArfGAP1 is required, we cannot assess directly if the amount of GTP-bound, active Lrrk increases in border cells and hence formally demonstrate that ArfGAP1 is required to inactivate Lrrk.

Furthermore, the tracking of RTKs in border cells is always limited to the use of the 4G10 antibody that recognizes all phosphorylated tyrosines. Although this tool has been validated and is standardly used in border cells (e.g.,<sup>18,19,24</sup>), it would be important in the long run to develop tools to directly detect PVR and EGFR, the two main receptors guiding border cell migration. Indeed, their distribution might be slightly different than the pattern obtained with 4G10, and it is also possible that they are differently regulated.

### STAR★METHODS

Detailed methods are provided in the online version of this paper and include the following:

- KEY RESOURCES TABLE
- RESOURCE AVAILABILITY
  - Lead contact
  - Materials availability
  - Data and code availability
- EXPERIMENTAL MODEL AND STUDY PARTICIPANT DETAILS
- METHOD DETAILS
  - Cloning
  - Immunofluorescence
  - Image acquisition and quantitative analysis
  - Live imaging and quantification
  - Migration quantification
- QUANTIFICATION AND STATISTICAL ANALYSIS
  - Statistical analysis

### SUPPLEMENTAL INFORMATION

Supplemental information can be found online at <https://doi.org/10.1016/j.isci.2023.107467>.

### ACKNOWLEDGMENTS

We thank the Bloomington Stock Collection and the Vienna Drosophila RNAi Center for fly stocks. We thank M. Gonzalez-Gaitan, J.A. Knoblich, S. Luschnig, T. Harris and C.T. Chien for their generosity in sharing reagents. We thank C. Charbonneau for technical assistance and the entire Emery lab for helpful discussions. This work was supported by grants from the Canadian Institutes of Health Research (CIHR; PJT - 175093) and the Natural Sciences and Engineering Research Council of Canada to G.E. A.B. held a doctoral scholarship from Institute for Research in Immunology and Cancer and from Molecular Biology Program of the University of Montreal. C.Z. held a doctoral scholarship from Fonds de Recherche du Québec - Santé (FRQS).

### AUTHOR CONTRIBUTIONS

Conceptualization, A.B. and G.E.; Methodology, A.B. and G.E.; Investigation, A.B. and C.Z.; Formal Analysis, A.B. and C.Z.; Writing – Original Draft, A.B. and G.E.; Writing – Review and Editing, A.B. and G.E.; Supervision, G.E.; Funding Acquisition, G.E.

### DECLARATION OF INTERESTS

The authors declare they have no competing interests.

## INCLUSION AND DIVERSITY

We support inclusive, diverse, and equitable conduct of research.

Received: September 20, 2022

Revised: June 21, 2023

Accepted: July 21, 2023

Published: July 25, 2023

## REFERENCES

- SenGupta, S., Parent, C.A., and Bear, J.E. (2021). The principles of directed cell migration. *Nat. Rev. Mol. Cell Biol.* 22, 529–547. <https://doi.org/10.1038/s41580-021-00366-6>.
- Haeger, A., Wolf, K., Zegers, M.M., and Friedl, P. (2015). Collective cell migration: guidance principles and hierarchies. *Trends Cell Biol.* 25, 556–566. <https://doi.org/10.1016/j.tcb.2015.06.003>.
- Heasman, S.J., and Ridley, A.J. (2008). Mammalian Rho GTPases: new insights into their functions from *in vivo* studies. *Nat. Rev. Mol. Cell Biol.* 9, 690–701. <https://doi.org/10.1038/nrm2476>.
- Peercy, B.E., and Starz-Gaiano, M. (2020). Clustered cell migration: Modeling the model system of *Drosophila* border cells. *Semin. Cell Dev. Biol.* 100, 167–176. <https://doi.org/10.1016/j.semcdb.2019.11.010>.
- Capuana, L., Boström, A., and Etienne-Manneville, S. (2020). Multicellular scale front-to-rear polarity in collective migration. *Curr. Opin. Cell Biol.* 62, 114–122. <https://doi.org/10.1016/j.cceb.2019.10.001>.
- Montell, D.J. (2003). Border-cell migration: the race is on. *Nat. Rev. Mol. Cell Biol.* 4, 13–24. <https://doi.org/10.1038/nrm1006>.
- Montell, D.J., Yoon, W.H., and Starz-Gaiano, M. (2012). Group choreography: mechanisms orchestrating the collective movement of border cells. *Nat. Rev. Mol. Cell Biol.* 13, 631–645. <https://doi.org/10.1038/nrm3433>.
- Duchek, P., and Rørth, P. (2001). Guidance of cell migration by EGF receptor signaling during *Drosophila* oogenesis. *Science* 291, 131–133. <https://doi.org/10.1126/science.291.5501.131>.
- Duchek, P., Somogyi, K., Jékely, G., Beccari, S., and Rørth, P. (2001). Guidance of cell migration by the *Drosophila* PDGF/VEGF receptor. *Cell* 107, 17–26. [https://doi.org/10.1016/S0092-8674\(01\)00502-5](https://doi.org/10.1016/S0092-8674(01)00502-5).
- McDonald, J.A., Pinheiro, E.M., and Montell, D.J. (2003). PVF1, a PDGF/VEGF homolog, is sufficient to guide border cells and interacts genetically with Taiman. *Development* 130, 3469–3478. <https://doi.org/10.1242/dev.00574>.
- McDonald, J.A., Pinheiro, E.M., Kadlec, L., Schubach, T., and Montell, D.J. (2006). Multiple EGFR ligands participate in guiding migrating border cells. *Dev. Biol.* 296, 94–103. <https://doi.org/10.1016/j.ydbio.2006.04.438>.
- Fernández-Espartero, C.H., Ramel, D., Farago, M., Malartre, M., Luque, C.M., Limanovich, S., Katzav, S., Emery, G., and Martín-Bermudo, M.D. (2013). GTP exchange factor Vav regulates guided cell migration by coupling guidance receptor signalling to local Rac activation. *J. Cell Sci.* 126, 2285–2293. <https://doi.org/10.1242/jcs.124438>.
- Plutoni, C., Keil, S., Zeledon, C., Delsin, L.E.A., Decelle, B., Roux, P.P., Carréno, S., and Emery, G. (2019). Misshapen coordinates protrusion restriction and actomyosin contractility during collective cell migration. *Nat. Commun.* 10, 3940. <https://doi.org/10.1038/s41467-019-11963-7>.
- Ramel, D., Wang, X., Laflamme, C., Montell, D.J., and Emery, G. (2013). Rab11 regulates cell-cell communication during collective cell movements. *Nat. Cell Biol.* 15, 317–324. <https://doi.org/10.1038/ncb2681>.
- Wang, H., Guo, X., Wang, X., Wang, X., and Chen, J. (2020). Supracellular Actomyosin Mediates Cell-Cell Communication and Shapes Collective Migratory Morphology. *iScience* 23, 101204. <https://doi.org/10.1016/j.isci.2020.101204>.
- Mishra, A.K., Mondo, J.A., Campanale, J.P., and Montell, D.J. (2019). Coordination of protrusion dynamics within and between collectively migrating border cells by myosin II. *Mol. Biol. Cell* 30, 2490–2502. <https://doi.org/10.1091/mbc.E19-02-0124>.
- Roberto, G.M., and Emery, G. (2022). Directing with restraint: Mechanisms of protrusion restriction in collective cell migrations. *Semin. Cell Dev. Biol.* 129, 75–81. <https://doi.org/10.1016/j.semcdb.2022.03.037>.
- Assaker, G., Ramel, D., Wculek, S.K., González-Gaitán, M., and Emery, G. (2010). Spatial restriction of receptor tyrosine kinase activity through a polarized endocytic cycle controls border cell migration. *Proc. Natl. Acad. Sci. USA.* 107, 22558–22563. <https://doi.org/10.1073/pnas.1010795108>.
- Laflamme, C., Assaker, G., Ramel, D., Dorn, J.F., She, D., Maddox, P.S., and Emery, G. (2012). Evi5 promotes collective cell migration through its Rab-GAP activity. *J. Cell Biol.* 198, 57–67. <https://doi.org/10.1083/jcb.201112114>.
- Zeledon, C., Sun, X., Plutoni, C., and Emery, G. (2019). The ArfGAP Drongo Promotes Actomyosin Contractility during Collective Cell Migration by Releasing Myosin Phosphatase from the Trailing Edge. *Cell Rep.* 28, 3238–3248.e3. <https://doi.org/10.1016/j.celrep.2019.08.044>.
- Cobrerros-Reguera, L., Fernández-Miñán, A., Fernández-Espartero, C.H., López-Schier, H., González-Reyes, A., and Martín-Bermudo, M.D. (2010). The Ste20 kinase misshapen is essential for the invasive behaviour of ovarian epithelial cells in *Drosophila*. *EMBO Rep.* 11, 943–949. <https://doi.org/10.1038/embor.2010.156>.
- Janssens, K., Sung, H.H., and Rørth, P. (2010). Direct detection of guidance receptor activity during border cell migration. *Proc. Natl. Acad. Sci. USA.* 107, 7323–7328. <https://doi.org/10.1073/pnas.0915075107>.
- Wan, P., Wang, D., Luo, J., Chu, D., Wang, H., Zhang, L., and Chen, J. (2013). Guidance receptor promotes the asymmetric distribution of exocyst and recycling endosome during collective cell migration. *Development* 140, 4797–4806. <https://doi.org/10.1242/dev.094979>.
- Jékely, G., Sung, H.H., Luque, C.M., and Rørth, P. (2005). Regulators of endocytosis maintain localized receptor tyrosine kinase signaling in guided migration. *Dev. Cell* 9, 197–207. <https://doi.org/10.1016/j.devcel.2005.06.004>.
- Caldieri, G., Malabarba, M.G., Di Fiore, P.P., and Sigismund, S. (2018). EGFR Trafficking in Physiology and Cancer. *Prog. Mol. Subcell. Biol.* 57, 235–272. [https://doi.org/10.1007/978-3-319-96704-2\\_9](https://doi.org/10.1007/978-3-319-96704-2_9).
- Adarska, P., Wong-Dilworth, L., and Bottanelli, F. (2021). ARF GTPases and Their Ubiquitous Role in Intracellular Trafficking Beyond the Golgi. *Front. Cell Dev. Biol.* 9, 679046. <https://doi.org/10.3389/fcell.2021.679046>.
- Rodrigues, F.F., and Harris, T.J.C. (2019). Key roles of Arf small G proteins and biosynthetic trafficking for animal development. *Small GTPases* 10, 403–410. <https://doi.org/10.1080/21541248.2017.1304854>.
- Jackson, C.L., and Bouvet, S. (2014). Arfs at a glance. *J. Cell Sci.* 127, 4103–4109. <https://doi.org/10.1242/jcs.144899>.
- Cukierman, E., Huber, I., Rotman, M., and Cassel, D. (1995). The ARF1 GTPase-activating protein: zinc finger motif and Golgi complex localization. *Science* 270, 1999–2002. <https://doi.org/10.1126/science.270.5244.1999>.
- Lee, S.Y., Yang, J.S., Hong, W., Premont, R.T., and Hsu, V.W. (2005). ARFGAP1 plays a central role in coupling COPI cargo sorting with vesicle formation. *J. Cell Biol.* 168, 281–290. <https://doi.org/10.1083/jcb.200404008>.
- Liu, W., Duden, R., Phair, R.D., and Lippincott-Schwartz, J. (2005). ArfGAP1 dynamics and its role in COPI coat assembly on Golgi membranes of living cells. *J. Cell Biol.* 168, 1053–1063. <https://doi.org/10.1083/jcb.200410142>.

32. Rodriguez-Fernandez, I.A., and Dell'Angelica, E.C. (2015). Identification of Atg2 and ArfGAP1 as Candidate Genetic Modifiers of the Eye Pigmentation Phenotype of Adaptor Protein-3 (AP-3) Mutants in *Drosophila melanogaster*. *PLoS One* 10, e0143026. <https://doi.org/10.1371/journal.pone.0143026>.
33. Raghu, P., Coessens, E., Manifava, M., Georgiev, P., Pettitt, T., Wood, E., Garcia-Murillas, I., Okkenhaug, H., Trivedi, D., Zhang, Q., et al. (2009). Rhabdomere biogenesis in *Drosophila* photoreceptors is acutely sensitive to phosphatidic acid levels. *J. Cell Biol.* 185, 129–145. <https://doi.org/10.1083/jcb.200807027>.
34. Khadilkar, R.J., Rodrigues, D., Mote, R.D., Sinha, A.R., Kulkarni, V., Magadi, S.S., and Inamdar, M.S. (2014). ARF1-GTP regulates Asrij to provide endocytic control of *Drosophila* blood cell homeostasis. *Proc. Natl. Acad. Sci. USA.* 111, 4898–4903. <https://doi.org/10.1073/pnas.1303559111>.
35. Armbruster, K., and Luschnig, S. (2012). The *Drosophila* Sec7 domain guanine nucleotide exchange factor protein Gartenzwerg localizes at the cis-Golgi and is essential for epithelial tube expansion. *J. Cell Sci.* 125, 1318–1328. <https://doi.org/10.1242/jcs.096263>.
36. Stafa, K., Trancikova, A., Webber, P.J., Glauser, L., West, A.B., and Moore, D.J. (2012). GTPase activity and neuronal toxicity of Parkinson's disease-associated LRRK2 is regulated by ArfGAP1. *PLoS Genet.* 8, e1002526. <https://doi.org/10.1371/journal.pgen.1002526>.
37. Xiong, Y., Yuan, C., Chen, R., Dawson, T.M., and Dawson, V.L. (2012). ArfGAP1 is a GTPase activating protein for LRRK2: reciprocal regulation of ArfGAP1 by LRRK2. *J. Neurosci.* 32, 3877–3886. <https://doi.org/10.1523/JNEUROSCI.4566-11.2012>.
38. Civiero, L., and Bubacco, L. (2012). Human leucine-rich repeat kinase 1 and 2: intersecting or unrelated functions? *Biochem. Soc. Trans.* 40, 1095–1101. <https://doi.org/10.1042/BST20120123>.
39. Usmani, A., Shavarebi, F., and Hiniker, A. (2021). The Cell Biology of LRRK2 in Parkinson's Disease. *Mol. Cell Biol.* 41, e00660-20. <https://doi.org/10.1128/MCB.00660-20>.
40. Zirin, J., Hu, Y., Liu, L., Yang-Zhou, D., Colbeth, R., Yan, D., Ewen-Campen, B., Tao, R., Vogt, E., VanNest, S., et al. (2020). Large-Scale Transgenic *Drosophila* Resource Collections for Loss- and Gain-of-Function Studies. *Genetics* 214, 755–767. <https://doi.org/10.1534/genetics.119.302964>.
41. Szafer, E., Pick, E., Rotman, M., Zuck, S., Huber, I., and Cassel, D. (2000). Role of coatamer and phospholipids in GTPase-activating protein-dependent hydrolysis of GTP by ADP-ribosylation factor-1. *J. Biol. Chem.* 275, 23615–23619. <https://doi.org/10.1074/jbc.M003171200>.
42. Bianco, A., Poukkala, M., Cliffe, A., Mathieu, J., Luque, C.M., Fulga, T.A., and Rørth, P. (2007). Two distinct modes of guidance signalling during collective migration of border cells. *Nature* 448, 362–365. <https://doi.org/10.1038/nature05965>.
43. Pinheiro, E.M., and Montell, D.J. (2004). Requirement for Par-6 and Bazooka in *Drosophila* border cell migration. *Development* 131, 5243–5251. <https://doi.org/10.1242/dev.01412>.
44. Li, Q., Shen, L., Xin, T., Xiang, W., Chen, W., Gao, Y., Zhu, M., Yu, L., and Li, M. (2009). Role of Scrib and Dlg in anterior-posterior patterning of the follicular epithelium during *Drosophila* oogenesis. *BMC Dev. Biol.* 9, 60. <https://doi.org/10.1186/1471-213X-9-60>.
45. Wang, H., Qiu, Z., Xu, Z., Chen, S.J., Luo, J., Wang, X., and Chen, J. (2018). aPKC is a key polarity determinant in coordinating the function of three distinct cell polarities during collective migration. *Development* 145, dev158444. <https://doi.org/10.1242/dev.158444>.
46. Niewiadomska, P., Godt, D., and Tepass, U. (1999). DE-Cadherin is required for intercellular motility during *Drosophila* oogenesis. *J. Cell Biol.* 144, 533–547. <https://doi.org/10.1083/jcb.144.3.533>.
47. Cai, D., Chen, S.C., Prasad, M., He, L., Wang, X., Choemmel-Cadamuro, V., Sawyer, J.K., Danuser, G., and Montell, D.J. (2014). Mechanical feedback through E-cadherin promotes direction sensing during collective cell migration. *Cell* 157, 1146–1159. <https://doi.org/10.1016/j.cell.2014.03.045>.
48. Han, D.D., Stein, D., and Stevens, L.M. (2000). Investigating the function of follicular subpopulations during *Drosophila* oogenesis through hormone-dependent enhancer-targeted cell ablation. *Development* 127, 573–583. <https://doi.org/10.1242/dev.127.3.573>.
49. Prasad, M., and Montell, D.J. (2007). Cellular and molecular mechanisms of border cell migration analyzed using time-lapse live-cell imaging. *Dev. Cell* 12, 997–1005. <https://doi.org/10.1016/j.devcel.2007.03.021>.
50. Wucherpfennig, T., Wilsch-Bräuninger, M., and González-Gaitán, M. (2003). Role of *Drosophila* Rab5 during endosomal trafficking at the synapse and evoked neurotransmitter release. *J. Cell Biol.* 161, 609–624. <https://doi.org/10.1083/jcb.200211087>.
51. Gillooly, D.J., Morrow, I.C., Lindsay, M., Gould, R., Bryant, N.J., Gaullier, J.M., Parton, R.G., and Stenmark, H. (2000). Localization of phosphatidylinositol 3-phosphate in yeast and mammalian cells. *EMBO J.* 19, 4577–4588. <https://doi.org/10.1093/emboj/19.17.4577>.
52. Jafar-Nejad, H., Andrews, H.K., Acar, M., Bayat, V., Wirtz-Peitz, F., Mehta, S.Q., Knoblich, J.A., and Bellen, H.J. (2005). Sec15, a component of the exocyst, promotes notch signaling during the asymmetric division of *Drosophila* sensory organ precursors. *Dev. Cell* 9, 351–363. <https://doi.org/10.1016/j.devcel.2005.06.010>.
53. Ishikawa, K., Nara, A., Matsumoto, K., and Hanafusa, H. (2012). EGFR-dependent phosphorylation of leucine-rich repeat kinase LRRK1 is important for proper endosomal trafficking of EGFR. *Mol. Biol. Cell* 23, 1294–1306. <https://doi.org/10.1091/mbc.E11-09-0780>.
54. Hanafusa, H., Ishikawa, K., Kedashiro, S., Saigo, T., Iemura, S.I., Natsume, T., Komada, M., Shibuya, H., Nara, A., and Matsumoto, K. (2011). Leucine-rich repeat kinase LRRK1 regulates endosomal trafficking of the EGFR receptor. *Nat. Commun.* 2, 158. <https://doi.org/10.1038/ncomms1161>.
55. Malik, A.U., Karapetsas, A., Nirujogi, R.S., Mathea, S., Chatterjee, D., Pal, P., Lis, P., Taylor, M., Purlyte, E., Gourlay, R., et al. (2021). Deciphering the LRRK code: LRRK1 and LRRK2 phosphorylate distinct Rab proteins and are regulated by diverse mechanisms. *Biochem. J.* 478, 553–578. <https://doi.org/10.1042/BCJ20200937>.
56. Gómez-Suaga, P., Rivero-Ríos, P., Fdez, E., Blanca Ramírez, M., Ferrer, I., Aiastui, A., López De Munain, A., and Hilfiker, S. (2014). LRRK2 delays degradative receptor trafficking by impeding late endosomal budding through decreasing Rab7 activity. *Hum. Mol. Genet.* 23, 6779–6796. <https://doi.org/10.1093/hmg/ddu395>.
57. Hanafusa, H., Yagi, T., Ikeda, H., Hisamoto, N., Nishioka, T., Kaibuchi, K., Shirakabe, K., and Matsumoto, K. (2019). LRRK1 phosphorylation of Rab7 at S72 links trafficking of EGFR-containing endosomes to its effector RILP. *J. Cell Sci.* 132, jcs228809. <https://doi.org/10.1242/jcs.228809>.
58. Dodson, M.W., Zhang, T., Jiang, C., Chen, S., and Guo, M. (2012). Roles of the *Drosophila* LRRK2 homolog in Rab7-dependent lysosomal positioning. *Hum. Mol. Genet.* 21, 1350–1363. <https://doi.org/10.1093/hmg/ddr573>.
59. Dietzl, G., Chen, D., Schnorrer, F., Su, K.C., Barinova, Y., Fellner, M., Gasser, B., Kinsey, K., Oettel, S., Scheiblauber, S., et al. (2007). A genome-wide transgenic RNAi library for conditional gene inactivation in *Drosophila*. *Nature* 448, 151–156. <https://doi.org/10.1038/nature05954>.
60. DeVorkin, L., and Gorski, S.M. (2014). Monitoring autophagy in *Drosophila* using fluorescent reporters in the UAS-GAL4 system. *Cold Spring Harb. Protoc.* 2014, 967–972. <https://doi.org/10.1101/pdb.prot080341>.
61. Lin, C.H., Li, H., Lee, Y.N., Cheng, Y.J., Wu, R.M., and Chien, C.T. (2015). Lrrk regulates the dynamic profile of dendritic Golgi outposts through the golgin Lava lamp. *J. Cell Biol.* 210, 471–483. <https://doi.org/10.1083/jcb.201411033>.

STAR★METHODS

KEY RESOURCES TABLE

REAGENT or RESOURCE	SOURCE	IDENTIFIER
<b>Antibodies</b>		
Mouse monoclonal anti-pTyr (clone 4G10)	Millipore Sigma	Cat#05-321; RRID:AB_309678
Rabbit polyclonal anti-pERM	Cell Signaling	Cat#3141S; RRID:AB_330232
Mouse monoclonal anti-Fasciclin III	DSHB	Cat#7G10; RRID:AB_528238
Rat monoclonal anti-DE cadherin	DSHB	Cat#DCAD2; RRID:AB_528120
Rabbit anti-Bazooka	gift from T. Harris (University of Toronto)	Yu and Harris, 2012 <sup>59</sup>
Mouse monoclonal anti-Discs Large	DSHB	Cat#4F3; RRID:AB_528203
Mouse monoclonal anti-Hrs	DSHB	Cat#Hrs27-4; RRID:AB_2618261
Mouse monoclonal anti-Flag M2	Sigma-Aldrich	Cat#F3165; RRID:AB_259529
LysoTracker RED DND-99	Invitrogen	Cat#L7528
Goat polyclonal anti-Mouse IgG (H+L) Highly Cross-adsorbed Antibody, Alexa Fluor 488 Conjugated	Invitrogen	Cat# A-11029; RRID:AB_2534088
Goat polyclonal anti-Mouse IgG (H+L) Highly Cross-adsorbed Antibody, Alexa Fluor 555 Conjugated	Invitrogen	Cat# A-21424; RRID:AB_141780
Goat polyclonal anti-Rabbit IgG (H+L) Cross-Adsorbed Secondary Antibody, Alexa Fluor 488	Invitrogen	Cat# A-11008; RRID:AB_143165
Goat polyclonal anti-Rabbit IgG (H+L) Antibody, Alexa Fluor 594 Conjugated	Invitrogen	Cat# A-11012; RRID:AB_141359
Goat polyclonal anti-Rat IgG (H+L) Antibody, Alexa Fluor 488 Conjugated	Invitrogen	Cat# A-11006; RRID:AB_141373
<b>Critical commercial assays</b>		
DNeasy Blood & Tissue Kit	QIAGEN	Cat#69504
<b>Experimental models: Organisms/strains</b>		
<i>Drosophila melanogaster</i> : UAS-Lifeact-GFP: y1 w*; P{UAS-Lifeact-GFP}VIE-260B	Bloomington Drosophila Stock Center	BDSC #35544; RRID:BDSC_35544
<i>Drosophila melanogaster</i> : c306-GAL4: P{w [+mW.hs]=GawB}c306, w[11118]	Bloomington Drosophila Stock Center	BDSC #3743; RRID:BDSC_3743
<i>Drosophila melanogaster</i> : UAS-RNAi mCherry: y[1] sc[*] v[1] sev[21]; P{y[+t7.7] v[+t1.8] =VALIUM20-mCherry}attP2	Bloomington Drosophila Stock Center	BDSC #35785; RRID:BDSC_35785
<i>Drosophila melanogaster</i> : UAS-Lrrk-IR #1: y[1] v[1]; P{y[+t7.7] v[+t1.8]=TRiP.HMS01937} attP40	Bloomington Drosophila Stock Center	BDSC #39019; RRID:BDSC_39019
<i>Drosophila melanogaster</i> : nos-Cas9: y[1] sc[*] v[1] sev[21]; P{y[+t7.7] v[+t1.8]=nos-Cas9.R} attP40	Bloomington Drosophila Stock Center	BDSC #78781; RRID:BDSC_78781
<i>Drosophila melanogaster</i> : sgRNA ArfGAP1: y [1] v[1]; P{y[+t7.7] v[+t1.8]=TKO.GS04820} attP40	Bloomington Drosophila Stock Center	BDSC #81490; RRID:BDSC_81490
<i>Drosophila melanogaster</i> : UAS-Hrs-IR #2: y[1] sc[*] v[1] sev[21]; P{y[+t7.7] v[+t1.8] =TRiP.HMS00840}attP2	Bloomington Drosophila Stock Center	BDSC #34086; RRID:BDSC_34086

(Continued on next page)

**Continued**

REAGENT or RESOURCE	SOURCE	IDENTIFIER
<i>Drosophila melanogaster</i> : UAS-Lrrk-IR #2: y[1] sc[*] v[1] sev[21]; P{y[+7.7] v[+1.8]} =TRiP.GL00136jattP2/TM3, Sb[1]	Bloomington Drosophila Stock Center	BDSC #35249; RRID:BDSC_35249
<i>Drosophila melanogaster</i> : UAS-Lrrk-IR #3: y[1] sc[*] v[1] sev[21]; P{y[+7.7] v[+1.8]} =TRiP.HMS00456jattP2	Bloomington Drosophila Stock Center	BDSC #32457; RRID:BDSC_32457
<i>Drosophila melanogaster</i> : ArfGAP1-IR: UAS-RNAi ArfGAP1	Vienna Drosophila Resource Center	VDRC #26460
<i>Drosophila melanogaster</i> : UAS-Cbl-IR	Vienna Drosophila Resource Center	VDRC #330142
<i>Drosophila melanogaster</i> : UAS-Hrs-IR #1	Vienna Drosophila Resource Center	VDRC #330597
<i>Drosophila melanogaster</i> : ArfGAP1 <sup>5</sup>	This study	N/A
<i>Drosophila melanogaster</i> : UAS-ArfGAP1-mCherry	This study	N/A
<i>Drosophila melanogaster</i> : UAS-ArfGAP1 <sup>R50Q</sup> -mCherry	This study	N/A
<i>Drosophila melanogaster</i> : Fos-pse-ArfGAP1	This study	N/A
<i>Drosophila melanogaster</i> : UAS-GFP-myc2xFYVE/TM3	gift from M. Gonzalez-Gaitan (Université de Genève)	Wucherpfennig et al. <sup>50</sup>
<i>Drosophila melanogaster</i> : UAS-GFP-Rab5/TM3	gift from M. Gonzalez-Gaitan (Université de Genève)	Wucherpfennig et al. <sup>50</sup>
<i>Drosophila melanogaster</i> : UAS-GFP-Rab7/CyO	gift from M. Gonzalez-Gaitan (Université de Genève)	Entchev et al. <sup>60</sup>
<i>Drosophila melanogaster</i> : UAS-eGFP-sec15/TM3	gift from J.A. Knoblich (Institute of Molecular Biotechnology of the Austrian Academy of Sciences)	Jafar-Nejad et al. <sup>52</sup>
<i>Drosophila melanogaster</i> : UAS-GalT-GFP	gift from S. Luschnig (WMU Munster)	Armbruster and Luschnig <sup>35</sup>
<i>Drosophila melanogaster</i> : UAS-Flag-dLrrk	gift from C.T. Chien (Academia Sinica)	Lin et al. <sup>61</sup>
<b>Oligonucleotides</b>		
Forward primer for the cloning ArfGAP1 into pDONR221: GGGGACAAGTTTG TACAAAAAAGCAGGCTTACCATGGCGAG TCCCAGAACGCG	This study	N/A
Reverse primer for the cloning ArfGAP1 into pDONR221: GGGGACCACTTTG TACAAGAAAGCTGGGTCGTTCA TCAGCAGATTCCAGG	This study	N/A
Primer 1 to generate ArfGAP1 <sup>R50Q</sup> : TGCACGCCAGACTCTGATGCTTGCC GGAG	This study	N/A
Primer 2 to generate ArfGAP1 <sup>R50Q</sup> : CTCCGGCAAGCATCAGAGTCTGGGCG TGCA	This study	N/A
Forward primer for the sequencing of ArfGAP1: GCGCCAGCGTCAGCAAAGTTTCATTAGC	This study	N/A
Reverse primer for the sequencing of ArfGAP1: CCTCCTTGAGATCCCAGCTCTTGCCC	This study	N/A
<b>Recombinant DNA</b>		
fosmid containing the ArfGAP1 ortholog from <i>Drosophila pseudoobscura</i>	Max Planck Institute of Molecular Cell Biology and Genetics (TransgeneOme Unit)	FlyFos062046

(Continued on next page)

**Continued**

REAGENT or RESOURCE	SOURCE	IDENTIFIER
Software and algorithms		
ImageJ	National Institutes of Health	RRID:SCR_003070 <a href="https://imagej.net/">https://imagej.net/</a>
Imaris	N/A	RRID:SCR_007370 <a href="http://www.bitplane.com/imaris/imaris">http://www.bitplane.com/imaris/imaris</a>
Chemotaxis and migration tool	Ibidi	RRID:SCR_022708 <a href="https://ibidi.com/chemotaxis-analysis/171-chemotaxis-and-migration-tool.html">https://ibidi.com/chemotaxis-analysis/171-chemotaxis-and-migration-tool.html</a>
GraphPad Prism	N/A	RRID:SCR_002798 <a href="http://www.graphpad.com/">http://www.graphpad.com/</a>

**RESOURCE AVAILABILITY****Lead contact**

Further information and requests for resources and reagents should be directed to and will be fulfilled by the lead contact, Gregory Emery ([gregory.emery@umontreal.ca](mailto:gregory.emery@umontreal.ca)).

**Materials availability**

This study generated fly lines expressing mCherry tagged ArfGAP1 and ArfGAP1e under the UAS promoter, a fly line with the mutated allele of ArfGAP1 (*ArfGAP1<sup>5</sup>*) and a fly line with a genomic fragment containing the *D.pseudoobscura* ArfGAP1 for rescue experiments.

**Data and code availability**

- All data reported in this paper will be shared by the [lead contact](#) upon request.
- This paper does not report original code.
- Any additional information required to reanalyze the data reported in this paper is available from the [lead contact](#) upon request.

**EXPERIMENTAL MODEL AND STUDY PARTICIPANT DETAILS**

Crosses were performed at 25°C and flies were incubated at 29°C for 48h before dissection. Knockdown and rescue experiments were performed with the c306-GAL4 driver. This driver expresses specifically in border cells. As we study migration in the ovary, the experiments were conducted in females. Transgenic flies were generated by BestGene Inc. The *ArfGAP1<sup>5</sup>* allele was generated by CRISPR using the TRiP-CRISPR Knockout stocks: nos-Cas9 (#78781) and sgRNA ArfGAP1 (#81490) obtained from the Bloomington Stock Collection. To identify the sequence alterations, we isolated DNA using the QIAGEN DNeasy Blood & Tissue Kit (QIAGEN, Hilden, Germany), amplified it by RT-PCR and sequenced the targeted site using 5'-GCGCCAGCGTCAGCAAAGTTT CATTAGC-3' as forward primer and 5'CCTCCTTGAGATCCCAGCTCTTGCCC3' as reverse primer.

The following stocks were obtained from the Bloomington Drosophila Stock Center: c306-GAL4 (#3743), UAS-Lifeact-GFP (#35544), UAS-RNAi mCherry (#35785), UAS-RNAi Hrs#2 (#34086), UAS-RNAi Lrrk (#39019), UAS-RNAi Lrrk#2 (#35249), UAS-RNAi Lrrk#3 (#32457). The fly lines: UAS-RNAi ArfGAP1 (#26460), UAS-RNAi Cbl (#330142) and UAS-RNAi Hrs (#330597) were obtained from the Vienna Drosophila RNAi Center.<sup>59</sup> UAS-GFP-myc2xFYVE/TM3, UAS-GFP-Rab5/TM3, UAS-GFP-Rab7/CyO were obtained from the group of M. Gonzalez-Gaitan (Department of Biochemistry, Université de Genève). UAS-eGFP-sec15/TM3 was obtained from the group of J.A. Knoblich (Institute of Molecular Biotechnology of the Austrian Academy of Sciences). UAS-GalT-GFP was obtained from the group of S. Luschnig (WMU Munster) (Armbruster and Luschnig, 2012). UAS-Flag-dLrrk was obtained from the group of C.T. Chien (Academia Sinica) (Lin et al., 2015).

**METHOD DETAILS****Cloning**

ArfGAP1 was cloned from a cDNA clone obtained from the Berkeley Drosophila Genome Project (RE63354). 5'-GGGGACAAGTTTGTACAAAAAAGCAGGCTTACCATGGCGAGTCCAGAACGCG-3' (forward primer)

and 5'-GGGGACCACTTTGTACAAGAAAGCTGGGTCGTTTCATCAGCAGATTCCAGG-3' (reverse primer) were used to amplify the sequence, which was inserted in a Gateway vector pDONR221. ArfGAP1 sequence was later inserted in a destination vector (pDest29) to obtain ArfGAP1-mCherry under the control of the UAS promoter. ArfGAP1<sup>R50Q</sup>-mCherry was generated by Quickchange mutagenesis using 5'-TGCACGCCAGAC TCTGATGCTTGCCGGAG-3' and 5'-CTCCGGCAAGCATCAGAGTCTGGGCGTGCA-3' primers. The fosmid containing the ArfGAP1 ortholog from *Drosophila pseudoobscura* was obtained from the Max Planck Institute of Molecular Cell Biology and Genetics (TransgeneOme Unit).

### Immunofluorescence

Ovaries were dissected in PBS (Phosphate Buffered Saline) and fixed in 200 $\mu$ L of paraformaldehyde 4% in PBS for 20min. After 3 washes in 200 $\mu$ L of Triton X-100 0.3% in PBS, ovaries were incubated in 200 $\mu$ L of bovine serum albumin (BSA) 2% + Triton X-100 0.3% in PBS for 1-3h under agitation at room temperature. Then, ovaries were incubated overnight at 4°C under agitation with the primary antibody (anti-pTyr (4G10) (05-321, Millipore Sigma, 1:40), anti-pERM (3141S, Cell Signaling, 1:100), anti-Fasciclin III (7G10, DSHB, 1:100), anti-DE cadherin (DCAD2, DSHB, 1:50), anti-Bazooka (gift from T.Harris lab, University of Toronto, 1:1500), anti-Discs Large (4F3, DSHB, 1:100), anti-Hrs (27-4-s, DSHB, 1:100) or anti-Flag M2 (F3165, Sigma-Aldrich, 1 :1000)) diluted in BSA 2% + Triton 0.3% in PBS. The next day, after 2 short washes and 2 20min washes under agitation with Triton 0.3% in PBS, ovaries were incubated during 1-3h under agitation at room temperature with secondary antibody (anti-mouse (A11029 or A21424, Invitrogen, 1:500), anti-rabbit (A11008 or A11012, Invitrogen, 1:250) or anti-rat (A11006, Invitrogen, 1:400), Phalloidin (A22287, Invitrogen, 1:1000) and DAPI (D8417-10MG, Sigma, 1:10 000)) diluted in BSA 2% + Triton 0.3% in PBS. Then, ovaries were washed again 2 times fast and 2 times during 20min under agitation before mounting on slides with Vectashield (H-1000, Vector Laboratories).

The protocol for staining with LysoTracker RED DND-99 (L7528, Invitrogen) was adapted from DeVorkin and Gorski (2016).<sup>60</sup> Ovaries were dissected in PBS 1X and incubated in 200 $\mu$ L of 50 $\mu$ M LysoTracker RED for 3min in the dark. Then, ovaries were washed 3 times 5min in 200 $\mu$ L of PBS 1X and fixed in 200 $\mu$ L of PFA 4% during 20min protected from light and subsequent steps were performed as previously described.

### Image acquisition and quantitative analysis

Images were acquired using a laser scanning confocal microscope LSM 700 (Carl Zeiss) or a Leica TCS SP8 (Leica Microsystems). To be consistent, clusters were quantified at stage 9, before they reached 25% of their migration path, ideally immediately after they rounded up and they started or complete their detachment from the follicular epithelium.

Mean pTyr fluorescence intensity was quantified using the ratio of mean pTyr intensity at the membrane at the front (defined as a line following the periphery of the cluster, as detected by actin labeling, and covering approximately 1/3 of the posterior part of the cluster based on the anteroposterior axis of the egg chamber), normalized to the signal between nurse cells (BC/NC) in three consecutive frames from a z-scan separated by 1 $\mu$ m using original images and the ImageJ software (National Institutes of Health). Lifeact-GFP or Phalloidin staining were used to determine the periphery of the cluster. Number of pTyr positive puncta were quantified by manually counting in three consecutive frames from a z-scan separated by 1 $\mu$ m. GFP-Rab7 mean intensity was measured on the entire cluster in three consecutive frames from a z-scan separated by 1 $\mu$ m. pMoesin mean intensity was quantified using the ratio of pMoesin mean fluorescence intensity at the cluster periphery, normalized to the signal between nurse cells (BC/NC) in three consecutive frames from a z-scan separated by 1 $\mu$ m. For all analyses, we used the z-scan containing the two polar cells as a central plan. The background, determined outside the egg chamber, was systematically subtracted from the fluorescence intensities determined. Only images with a signal in the linear range were considered for quantification. Intensity of the pTyr signal within Rab7-positive structures, volume, number and position of GFP-Rab7, LysoTracker RED and Sec15 vesicles were analyzed using the "Spot" function on Imaris (Bitplane), on an entire z-scan recorded with frames separated by 1 $\mu$ m. GalT-GFP structures were quantified by manually setting a threshold and automatic counting using the Analyze particles plugin in ImageJ, on a z-projection of five consecutive focal planes separated by 0.5 $\mu$ m.

### Live imaging and quantification

Dissection and primary culture of ovaries expressing LifeAct-GFP were performed as previously described (Prasad et al., 2007). Egg chambers were isolated and cultured in Schneider's medium containing 200 $\mu$ g/ml of insulin and 15% FBS for live imaging. A z-scan of 3 images separated by 3 $\mu$ m was acquired every 2min

over the course of 4 to 6 hours using a spinning disk confocal microscope (Zeiss). For rendering, they were processed on the ImageJ software using the “Maximum Intensity Z-projection” and the “Contrast and Brightness” function. Drift due to egg chamber movement was corrected on the time-lapse recording of one control border cell cluster using the “TurboReg” plugin in ImageJ. Manual cell tracking and x/y position recording of clusters were performed by using the “Manual Tracking” plugin in ImageJ. Accumulated distance, euclidean distance, directionality (euclidean distance/accumulated distance), and velocity were calculated with the x/y position recording from cluster tracking using the chemotaxis tool from Ibidi (<https://ibidi.com/chemotaxis-analysis/171-chemotaxis-and-migration-tool.html>). Total number of protrusions was manually quantified over 4 hours of time-lapse recording.

### Migration quantification

The migration index (M.I.) represents the relative distance, compared to the end of the migration path, migrated by BCs in the egg chamber at stage 10, whereas the completion index (C.I.) represents the ratio of clusters having completed migration, and both were calculated as previously described (Assaker et al., 2010). The Migration Index (M.I.) was calculated with the following formula:  $(0 \cdot n(0\%) + 0,25 \cdot n(25\%) + 0,5 \cdot n(50\%) + 0,75 \cdot n(75\%) + 1 \cdot n(100\%)) / n(\text{total})$ . The Completion Index (C.I.) corresponds to the number of egg chambers where the migration was completed divided by the total number of egg chambers:  $n(100\%) / n(\text{total})$ .  $n(100\%)$  corresponds to the number of egg chambers where the cluster reached the oocyte,  $n(75\%)$ , the number of chambers where the cluster migrated to 75% of the final distance, etc. and  $n(\text{total})$ , the total number of egg chambers.

## QUANTIFICATION AND STATISTICAL ANALYSIS

### Statistical analysis

Statistical comparisons of means were made by comparing each condition to the adequate control, using the unpaired non-parametric Mann-Whitney test or the Kruskal-Wallis test with Dunn’s correction for multiple comparisons using GraphPad Prism software. For Migration Indexes (M.I.) and Completion Indexes (C.I.), statistical comparisons of means were made by comparing each condition to the adequate control, using the unpaired One-way ANOVA test with correction for multiple comparisons using GraphPad Prism software.  $P < 0.05$  is represented by one star (\*),  $p < 0.01$  by two stars (\*\*),  $p < 0.001$  by three stars (\*\*\*) and  $p < 0.0001$  by four stars (\*\*\*\*). Mean values are quoted  $\pm$  SEM in figures.